Chatterjee, S. *et al.* (2012). *Géotechnique* **62**, No. 7, 573–582 [http://dx.doi.org/10.1680/geot.10.P.075]

The effects of penetration rate and strain softening on the vertical penetration resistance of seabed pipelines

S. CHATTERJEE*, M. F. RANDOLPH* and D. J. WHITE*

Offshore pipelines in deep water are generally laid directly on the seabed, without any additional stabilisation measures. Design parameters that determine the soil resistance to lateral and axial motion of the pipeline are a function of the amount of vertical embedment. However, this latter quantity is difficult to estimate, partly because of the effects of soil heave around the pipeline as it penetrates, and partly because the soil shear strength depends on the strain rate and the degree of softening as the soil is sheared and remoulded. In this paper, a large deformation finite-element approach was adopted to study pipe–soil interaction during vertical embedment of pipelines on the seabed. The simple Tresca soil model was modified to incorporate the combined effects of strain rate and softening. The present large deformation finite-element method was validated by comparing the results with data from centrifuge model tests. A parametric study was then performed, varying the strain rate and softening parameters to explore their effects on penetration resistance. Simple expressions for penetration resistance, incorporating the effects of strain rate and softening, have been developed. The effects of soil strength vertical heterogeneity and buoyancy have also been explored.

KEYWORDS: clays; numerical modelling; offshore engineering; shear strength

Les conduites d'hydrocarbures en eau profonde sont généralement posées directement sur le fond marin, sans aucune dispositif de stabilisation additionnel. Les paramètres d'étude déterminant la résistance du sol à des mouvements latéraux et axiaux de la conduite d'hydrocarbures sont fonction de l'encastrement vertical. Toutefois, cette dernière quantité est difficile à évaluer, en partie en raison des effets des soulèvements du sol autour de la conduite, lors de la pénétration de cette dernière, mais aussi du fait que la résistance du sol au cisaillement est fonction de la déformation plastique ainsi qu du degré d'adoucissement du sol cisaillé et remoulé. Dans la présente communication, on a adopté une méthode aux éléments finis pour déformations importantes afin d'étudier les interactions conduite/sol au cours de l'encastrement vertical des conduites dans le fond marin. On a modifié le simple modèle de sol Tresca afin d'incorporer les effets combinés de la déformation plastique et de l'adoucissement. On a validé a méthode aux éléments finis pour déformations importantes utilisée actuellement en comparant les résultats avec des données provenant des essais effectués sur maquette centrifuge. On a effectué ensuite une étude paramétrique, en variant les paramètres de déformation plastique et d'adoucissement, afin d'explorer leurs effets sur la résistance à la pénétration. On a développé de simples expressions pour la résistance à la pénétration, incorporant les effets de la déformation plastique et de l'adoucissement. On s'est également penché sur les effets de la résistance, de l'hétérogénéité verticale, et de la flottabilité du sol.

INTRODUCTION

Over the past two decades, offshore oil and gas facilities have gradually been extended from shallow-water fixed production systems to deep-water floating production systems. This has led to an increase in the relative importance of pipelines and risers in the design of offshore developments (Randolph & White, 2008a). Hydrocarbon products need to be transported safely within individual developments from wells to production facilities, between neighbouring fields and also to shore for treatment and processing. Unlike in shallow water, deep-water pipelines are generally laid directly on the seabed with no additional stabilisation measures. Accurate assessment of pipeline embedment is an important aspect of the design of deep-water pipelines in respect of on-bottom stability, lateral resistance to thermally induced buckles and axial resistance (Bruton *et al.*, 2006). Adopting conservatively low design values is not a safe approach because both high and low embedment, and the consequent high or low axial and lateral resistance, may work for or against a particular design consideration. Considerable cost savings can sometimes be justified by small refinements of these values (Randolph & White, 2008b).

The problem of pipeline embedment in fine-grained sediments has been an active topic of research for many years. Failure mechanisms and ultimate loads have been identified based on classical plasticity theory (Randolph & Houlsby, 1984; Murff *et al.*, 1989; Martin & Randolph, 2006; Randolph & White, 2008c), small-strain finite-element analyses (Aubeny *et al.*, 2005; Merifield *et al.*, 2008, 2009) and on model tests (Verley & Lund, 1995; Dingle *et al.*, 2008). Most of the theoretical studies assume the pipe to be 'wished-in-place' and do not capture the change in geometry during large amplitude deformation. Model tests performed in the centrifuge (Dingle *et al.*, 2008) are available, but they are too limited in number and confined to specific cases to provide general guidance. A recent study has demonstrated the potential of large deformation finite-element (LDFE) analysis for estimating the vertical and lateral response of pipes over significant displacements (Wang *et al.*, 2010).

Dynamic motions during pipe lay, and potential entrainment of water, result in a decrease in the shear strength of the seabed soil in the vicinity of the pipe. The amount of softening depends on the sensitivity and ductility of the soil. The effect of strain rate on the shear strength of soil has also been explored widely (Casagrande & Wilson, 1951;

Manuscript received 5 December 2010; revised manuscript accepted 22 September 2011. Published online ahead of print 16 May 2012. Discussion on this paper closes on 1 December 2012, for further details see p. ii.

* Centre for Offshore Foundation Systems, The University of Western Australia, Crawley, Australia.

Graham *et al.*, 1983; Lefebvre & LeBoeuf, 1987; Biscontin & Pestana, 2001; Lunne *et al.*, 2006; Lunne & Andersen, 2007; Yafrate & DeJong, 2007, Low *et al.*, 2008). The combined effects of strain rate and softening on the shear strength of the soil have been modelled recently in theoretical studies of deep penetration problems (Einav & Randolph, 2005; Zhou & Randolph, 2007, 2009) but this has yet to be applied to the problem of pipe penetration resistance.

The current paper presents the results of a detailed and systematic parametric study of the vertical embedment of pipelines in clay, incorporating the effects of strain rate and softening on soil strength. LDFE analysis has been performed using the commercial finite-element software Abaqus (Dassault Systèmes, 2007). The simple Tresca soil model was modified to account for the effects of strain rate and softening. Rate parameters, sensitivity and ductility of the soil were varied to investigate their effects on penetration resistance. The effects of soil strength non-homogeneity and buoyancy on the vertical resistance of pipelines were also evaluated. Simple relationships were then developed, expressing the non-dimensionalised vertical penetration resistance as a function of the normalised penetration.

LARGE DEFORMATION FINITE-ELEMENT MODEL

The LDFE method developed for this study is based on the 'Remeshing and interpolation technique with small strain' (RITSS, Hu & Randolph, 1998a, 1998b), but linked to a different finite-element package and incorporating improved techniques for interpolation of material stresses. RITSS is an extension of the arbitrary Lagrangian Eulerian (ALE, Ghosh & Kikuchi, 1991) method, incorporating periodic topological changes of the mesh. A series of small-strain Lagrangian calculations are performed, followed by remeshing of the deformed regime and interpolation of stress, strain and material properties from the old mesh to the new mesh. This is repeated until the required displacement is achieved.

The finite-element software Abaqus was used for making the model, mesh generation, analysis and post-processing. The problem was solved using a displacement-controlled approach. Following the RITSS method, the whole displacement is divided into a series of small displacement steps, typically of 1% of the pipe diameter in each step. Python, which is the in-built scripting language of Abaqus software, is used to execute different Abaqus functions. First, a Python script provides details of the model and generates the mesh for the first step. The model is used as input to Abaqus for standard analysis with very small displacement increments.

After completion of each step of standard analysis, the output database is post-processed with the help of another Python script. The coordinates of the nodes of the displaced model, and also stresses at integration points and reaction forces, are recorded. A Fortran subroutine was written to recover stresses from the Gauss points to the nodes of the triangular elements. The superconvergent patch recovery (SPR) technique (Zienkiewicz & Zhu, 1992) was used for stress recovery. Another Fortran subroutine was written to generate the boundary of the displaced soil regime. A further Python script was written to create the model and generate the mesh for the next step, which provides the input to Abaqus for standard analysis. Before the start of this step, the recovered stresses at the displaced nodes of the previous mesh are interpolated, with the help of a Fortran subroutine, to the new integration points of the remeshed structure. Then Abaqus's in-built user subroutine 'Sigini' is used to define the initial stresses at the Gauss points. In this manner, with a very small displacement in each step, the pipe is moved a significant distance by means of a series of small-strain analyses. The whole process is controlled by a master Fortran program, which repeatedly calls on Fortran subroutines and Python scripts to accomplish the analysis automatically without the intervention of the user (see the flow diagram in Fig. 1).

Mesh, boundary conditions and material model

A two-dimensional plane strain model was used (as shown in Fig. 2). The two side edges of the model were restrained horizontally but free to move vertically, whereas the bottom edge was restrained both vertically and horizontally. The pipe was considered as a rigid body. The two-dimensional (2D) plane strain element CPE6 of the Abaqus element library was used, which has three vertex nodes and three mid-side nodes. The optimal size of the model and mesh density were established after trying several options, and ensuring objective results were obtained. An incremental displacement, taken as 1% of the diameter of the pipe, was imposed at the centre of the pipe. This incremental displacement was verified to be small enough by running one set of analyses with an incremental displacement of 0·1% of the diameter and confirming negligible variation in the overall response. Contact between the pipe and the soil was simulated by defining the pipe surface as the master surface and

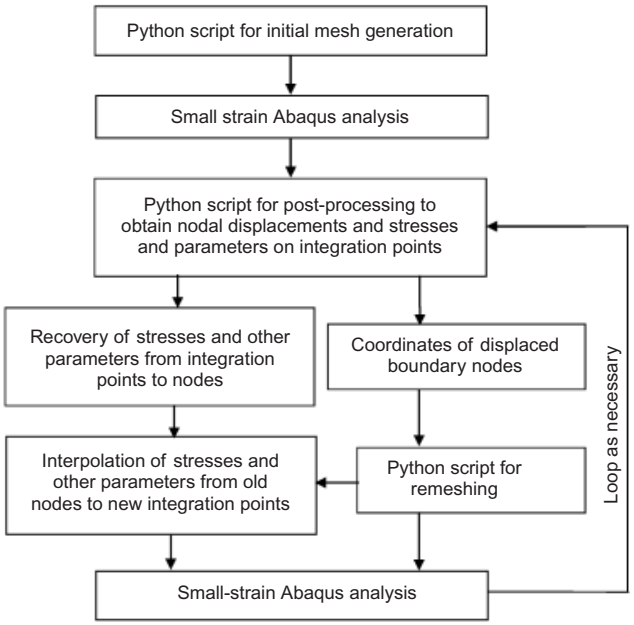

Fig. 1. Overall scheme of the LDFE method

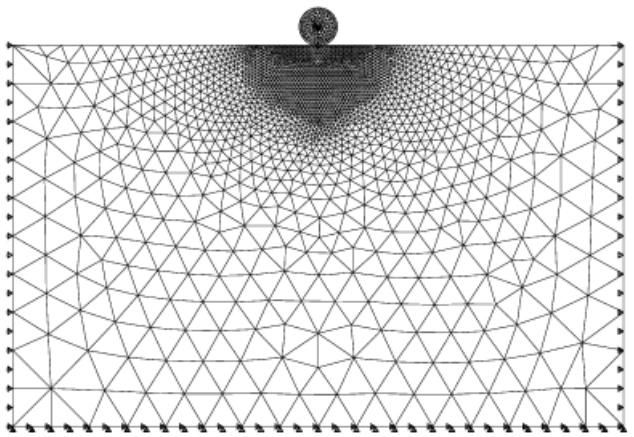

Fig. 2. Mesh and boundary conditions

the soil surface as the slave surface in Abaqus. For considering friction between pipe and soil, the penalty method in Abaqus was used, with the maximum shear stress at the interface, τ_{max} set as αs_{um}, where α is the interface roughness factor and s_{um} is the mudline shear strength of soil. In most cases, as detailed below, a value of $\alpha = 1/S_t$ was used where S_t is the sensitivity of the soil, corresponding to the ratio of the intact and remoulded values. As a result, the interface resistance was equal to the remoulded strength at the mudline. This approach is justified by the assumption that a thin layer of surficial soil is smeared onto the pipe surface and dragged downwards.

All the analyses were performed using an undrained total stress approach, based on the Mohr–Coulomb soil model with zero friction angle (equivalent to the simple Tresca model). For the elastic part of the linear-elastic–perfectly-plastic soil model, a Poisson's ratio of 0·499 (~0·5) was adopted to impose negligible volume change. The Young's modulus, E, of the soil was taken as 500 times the shear strength, s_u, at the given depth.

Strain rate and strain softening

The effects of strain rate and strain softening on shear strength were incorporated in the analysis according to the model suggested by previous researchers (Einav & Randolph, 2005; Zhou & Randolph, 2007). The simple elastic–perfectly plastic Tresca soil model was modified accordingly. At each remeshing and interpolation stage of the analysis, the shear strength of each element was modified to account for a reduction due to strain softening as well as an enhancement due to high strain rate, with the strength due to the combined effects given by

$$s_u = \left[1 + \mu \log\left(\frac{\max(\dot{\gamma}_{max}, \dot{\gamma}_{ref})}{\dot{\gamma}_{ref}}\right)\right] \times \left[\delta_{rem} + (1 - \delta_{rem})e^{-3\xi/\xi_{95}}\right] s_{u0} \quad (1)$$

The first part of this relationship captures the effect of strain rate, $\dot{\gamma}$, with the reference shear strain, $\dot{\gamma}_{ref}$, taken as 1%/h or 3×10^{-6} s^{-1} and the rate parameter, μ, giving the rate of strength increase per decade, taken in the range of 0·05–0·2 (Biscontin & Pestana, 2001; Lunne & Andersen, 2007). The maximum shear strain rate at a given location, $\dot{\gamma}_{max}$ is defined by

$$\dot{\gamma}_{max} = \frac{(\Delta\varepsilon_1 - \Delta\varepsilon_3)}{\delta/D}\frac{v_p}{D} \quad (2)$$

where $\Delta\varepsilon_1$ and $\Delta\varepsilon_3$ are major and minor principal strains, respectively, resulting from a displacement increment δ, D is the pipe diameter and v_p is the pipe velocity. The pipe velocity is used to identify the time period corresponding to each small-strain analysis (of a 1% D displacement increment, $\delta/D = 0{\cdot}01$).

The second part of equation (1) represents the effect of strain softening. Here, s_{u0} denotes the original shear strength at the reference shear strain rate prior to any softening, δ_{rem} is the ratio of fully remoulded and initial shear strength and hence is the inverse of sensitivity of soil. The sensitivity of the soil (S_t) typically ranges from 2 to 6 in the case of marine clays (Randolph, 2004). ξ is the accumulated absolute plastic shear strain at the Gauss point and ξ_{95} is the cumulative shear strain for 95% shear strength degradation, with typical value ranging from 10 to 50 (Randolph, 2004).

Validation of finite-element model

To validate the finite-element model, initially a set of parameters was chosen that matched those from a centrifuge modelling study (Dingle *et al.*, 2008). The prototype diameter of the pipe was $D = 0{\cdot}8$ m. Shear strength, s_{u0} at any depth z for this simulation was taken as $2{\cdot}3 + 3{\cdot}6z$ kPa (with z the equivalent prototype depth in m). The submerged (i.e. effective) unit weight of the kaolin clay was 6·5 kN/m^3. The sensitivity of the clay was considered as 3·2, reflecting results from cyclic T-bar tests. The friction ratio at the pipe–soil interface, α, was taken as equal to the inverse of sensitivity ($1/S_t = 0{\cdot}31$).

The pipe was penetrated down to a depth of 0·45 times the diameter of the pipe. The vertical reaction force during embedment, V, was non-dimensionalised by Ds_{u0}, with s_{u0} being the nominal intact (reference shear strain rate) shear strength of the soil at a level corresponding to the invert of the pipe. The measured and computed variations of normalised vertical resistance on the pipe, V/Ds_{u0}, with non-dimensionalised embedment, w/D, are plotted in Fig. 3. When the effects of strain rate and softening are not considered, the numerical results are quite different from the centrifuge data. If both strain rate and softening effects are taken into account, the computed response gives a good match with the centrifuge data (Fig. 3) and hence provides some validation of the LDFE approach.

It should be noted that there is some jaggedness in the LDFE results for normalised penetration resistance, which is generally not observed for small-strain analyses. This is partly due to the spatial variation (and small oscillations) in the softened and rate-dependent shear strength in the soil domain. Also, interpolation of the shear strength values and other quantities following remeshing contributes to the jaggedness.

PARAMETRIC STUDY

Details of the parameters chosen for the parametric study are shown in Table 1. A base case for rate and softening parameters were chosen with $v_p/D\dot{\gamma}_{ref} = 1000$, $\mu = 0{\cdot}1$, $S_t = 3$ and $\xi_{95} = 20$. The submerged unit weight of the soil, $\gamma' = 5$ kN/m^3 was considered for this case, since this is typical of deep water sediments. Keeping other parameters equal to this base case, one parameter was varied at a time (as in Table 1). The pipe diameter, D was taken as 0·5 m for all the cases, although all results are presented in normalised form and may be generalised to other diameters.

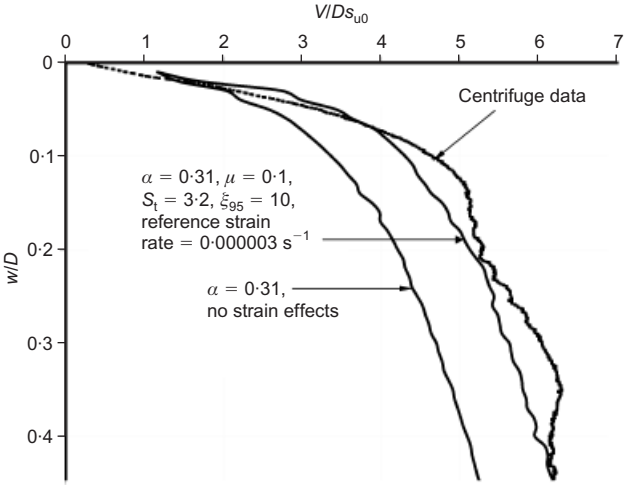

Fig. 3. Comparison with centrifuge result

Table 1. Parameters chosen for LDFE analyses

kD/s_{um}	$\gamma' D/s_{um}$	$v_p/D\dot{\gamma}_{ref}$	μ	S_t	ξ_{95}
0	0·25	0, 100, 1000, 10 000	0·1	3	20
0	0·25	1000	0, 0·05, 0·1, 0·15	3	20
0	0·25	1000	0·1	1, 2, 3, 6	20
0	0·25	1000	0·1	3	10, 20, 30
0	0·15, 0·25, 0·35	1000	0·1	3	20
1	1·25	0, 100, 1000, 10 000	0·1	3	20
1	1·25	1000	0, 0·05, 0·1, 0·15	3	20
1	1·25	1000	0·1	1, 2, 3, 6	20
1	1·25	1000	0·1	3	10, 20, 30
20	10	0, 100, 1000, 10 000	0·1	3	20
20	10	1000	0, 0·05, 0·1, 0·15	3	20
20	10	1000	0·1	1, 2, 3, 6	20
20	10	1000	0·1	3	10, 20, 30
20	6, 10, 14	1000	0·1	3	20

The shear strength of the soil, s_{u0}, at any depth z was assumed to vary according to the following linear variation

$$s_{u0} = s_{um} + kz \tag{3}$$

where s_{um} is the (intact) shear strength at the mudline and k is the shear strength gradient. Three values of κ ($= kD/s_{um}$) corresponding to 0 ($s_{um} = 10$ kPa and $k = 0$), 1 ($s_{um} = 2$ kPa and $k = 4$ kPa/m) and 20 ($s_{um} = 0{\cdot}25$ kPa and $k = 10$ kPa/m) were selected. The parametric study was repeated for these three values of κ. The maximum shear stress at the pipe–soil interface, τ_{max}, was taken as αs_{um}, with α equal to the inverse of the soil sensitivity. So, the maximum shear stress at the interface was actually the mudline remoulded shear strength. For each case, the pipe was penetrated down to a depth of 1D and vertical resistance forces were recorded at every increment of displacement (1% of the diameter of the pipe).

Effect of unit weight of soil

The vertical penetration resistance may be considered as the sum of the geotechnical resistance and a component due to buoyancy as the pipe becomes embedded within the soil. The geotechnical resistance is generally expressed as a power law (Aubeny *et al.*, 2005), so the total vertical resistance can be written as

$$\frac{V}{Ds_{u0}} = a\left(\frac{w}{D}\right)^b + f_b \frac{A_s}{D^2}\frac{\gamma' D}{s_{u0}} \tag{4}$$

where the first part of the right-hand side of the equation denotes geotechnical resistance (with power law parameters, a and b) and the second part represents the resistance due to buoyancy. A_s is the submerged cross-sectional area of the pipe, so that $A_s\gamma'$ is the (nominal) weight of soil displaced by the pipe. This is adjusted by a factor, f_b, which accounts for the enhanced buoyancy effect due to heave of the soil adjacent to the pipe. Merifield *et al.* (2009) found that f_b should be taken as around 1·5.

Keeping all other parameters as in the base case, the effect of unit weight was explored for soils with $\kappa = 0$ and $\kappa = 20$, taking submerged unit weights of 3, 5 and 7 kN/m^3. It is evident from Fig. 4 that the effect of unit weight is more pronounced for soil with a high value of κ; this is because the value of the non-dimensional parameter $\gamma' D/s_{um}$ lies in the range 0·15–0·35 for soil with $\kappa = 0$, whereas it is far higher, varying from 6 to 14, for soil with $\kappa = 20$.

To evaluate appropriate values of f_b for these cases, parallel sets of analyses were run with and without considering the self-weight of soil. This allowed the geotechnical resistance term to be isolated, and then the buoyancy term quantified by subtracting the geotechnical resistance from the total resistance for analyses that included self-weight of the soil. The value of f_b was thus deduced, albeit on the assumption that the geotechnical resistance is unchanged between the two cases, implying no significant change to the penetration mechanism.

As shown in Fig. 5(a), the average value of f_b was ~1·4

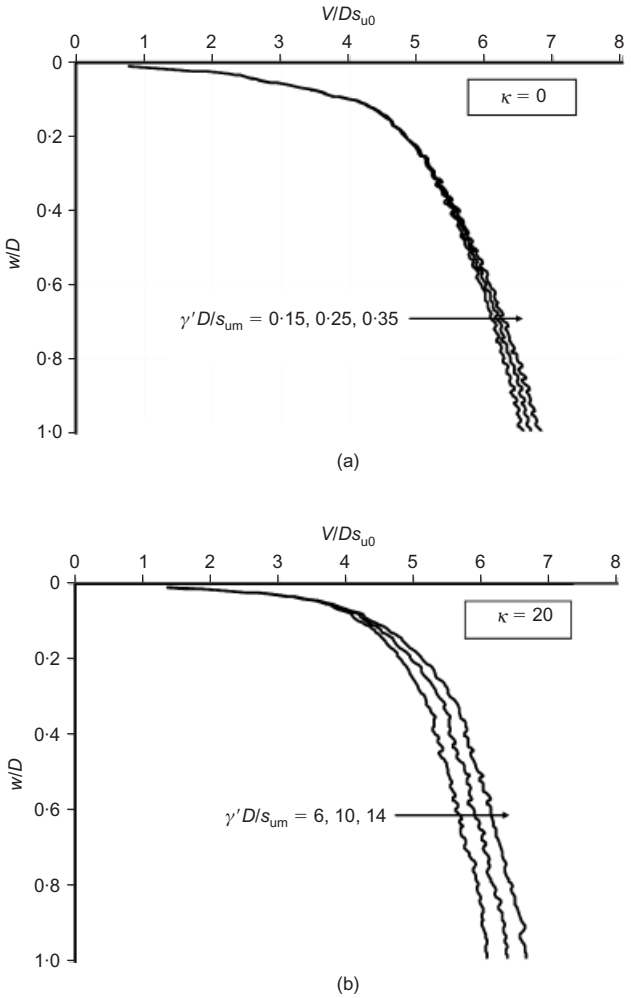

Fig. 4. Variation of vertical resistance for different submerged unit weights: (a) $\kappa = 0$; (b) $\kappa = 20$

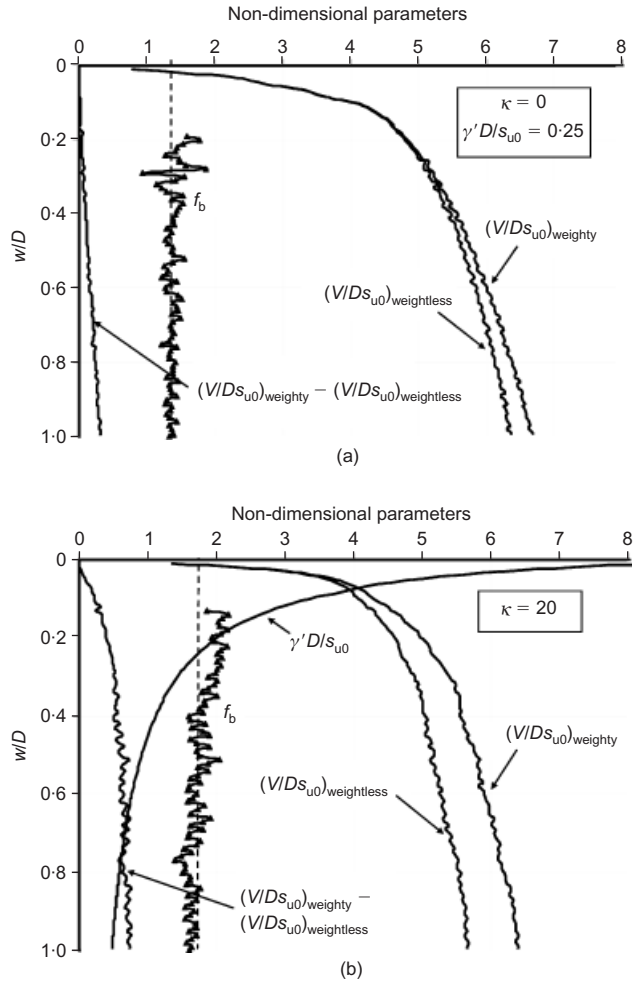

Fig. 5. Buoyancy factors f_b and other non-dimensional parameters with depth: (a) $\kappa = 0$; (b) $\kappa = 20$

for $\kappa = 0$. For soil with a high shear strength gradient ($\kappa = 20$), the average value of f_b was ~1·75 (Fig. 5(b)). A value of $f_b = 1{\cdot}5$ was obtained for $\kappa = 1$. The value of f_b is therefore a function of the shear strength gradient, k. It was found to vary linearly with the non-dimensional term $kD/s_{u,avg}$, where $s_{u,avg}$ is the average of shear strengths at the mudline and at a depth of one pipe diameter. Hence $kD/s_{u,avg}$ is bounded by 0 (for $k = 0$) and 2 (for $s_{um} = 0$). Fig. 6

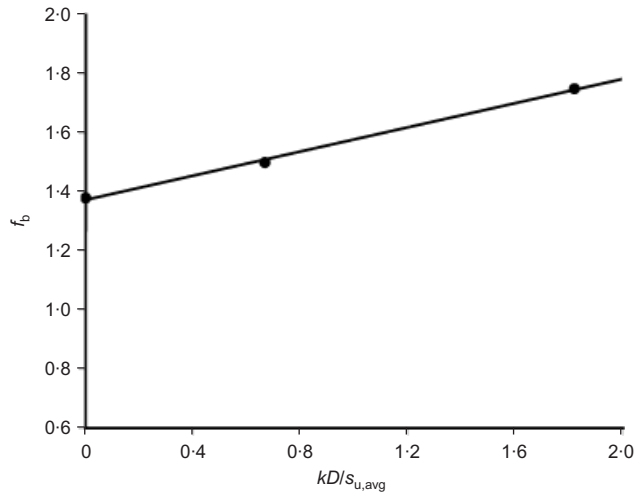

Fig. 6. Variation of buoyancy factor f_b with non-dimensional parameter $kD/s_{u,avg}$

shows the variation of f_b with $kD/s_{u,avg}$ for these three cases, with a simple linear trend line given by

$$f_b = 0{\cdot}2\left(kD/s_{u,avg}\right) + 1{\cdot}38 \quad (5)$$

Geotechnical resistance

It is convenient to quantify the geotechnical resistance using closed-form expressions suitable for routine design. Previously, power law relationships for the coefficients a and b in equation (4) have been obtained as a function of embedment (Aubeny *et al.*, 2005; Merifield *et al.*, 2009). Aubeny *et al.* (2005) gave power law fit coefficients for a 'wished-in-place' pipe with an open trench directly above it, and hence did not consider the change in geometry and formation of heave during continuous penetration. They also did not consider the effects of strain rate and softening. Merifield *et al.* (2009) gave results for 'pushed-in-place' pipes in uniform strength soil, and also did not consider the effects of strain rate and softening, or strength heterogeneity. Aubeny *et al.* (2005) gave results for two extreme values of κ (0 and ∞) and plotted a best-fit curve between them to predict the resistance for intermediate values of κ. The present study extends the previous work by establishing simple relationships for a range of κ values, but also accounting for rate effects and strain softening.

To compare results with Aubeny *et al.* (2005), the geotechnical resistances for different κ values in this study were averaged for displacements down to $0{\cdot}5D$ and fitted to a best-fit power law curve. Base case values for strain rate and softening parameters were adopted, as detailed earlier. Coefficients a and b of equation (4) for this base case and those from other researchers are shown in Table 2 for rough pipes only. The coefficients are applicable for the particular strain rate and softening parameters adopted in the base case. The effect of these parameters on the response is explored below and a more refined set of coefficients is derived.

Effect of normalised velocity, $v_p/D\dot{\gamma}_{ref}$

Three values of $v_p/D\dot{\gamma}_{ref}$, 100, 1000 and 10 000, were investigated for the parametric study with all other parameters similar to the base case. Soil with zero rate-dependency was also included for comparison. For $\kappa = 1$, the variation of vertical resistance for different values of $v_p/D\dot{\gamma}_{ref}$ is shown in Fig. 7(a). As the normalised velocity increases from 100 to 10 000, the vertical resistance increases by more than 20%. It is helpful to identify what equivalent soil strength, $s_{u0,eq}$, would reflect the effect of the increasing strain rate in the soil. Thus, instead of normalising V by Ds_{u0}, V was normalised by $Ds_{u0,eq}$, where

$$s_{u0,eq} = s_{u0}\left[1 + \mu \log\left(f_r v_p/D\dot{\gamma}_{ref}\right)\right] \quad (6)$$

The factor f_r reflects the average operative shear strain rate $\dot{\gamma}$ during each increment of pipe penetration relative to the normalised penetration rate, v_p/D. This factor was varied in order to find a suitable value to bring the various curves together, and a value of 0·7 was found to be appropriate. It can be seen from Fig. 7(b) that now points from all the above cases fall in a narrow band, implying that a representative operative strength during shallow pipe penetration is that at a strain rate corresponding to $0{\cdot}7v_p/D$.

Effect of rate parameter μ

The rate parameter, μ, was varied across values of 0·05, 0·1 and 0·15 to evaluate the effect on the vertical resistance. Fig. 8(a) shows the variation of vertical resistance with

Table 2. Comparison of coefficients *a* and *b* from literature and present study

	a	*b*	Comments
Aubeny *et al.* (2005)	6·73	0·29	Wished-in-place, no strain effects
Merifield *et al.* (2008)	7·4	0·4	Wished-in-place, no strain effects
Merifield *et al.* (2009)	7·1	0·33	Pushed-in-place, no strain effects
Base case of present study	6·81	0·25	Pushed-in-place, strain rate and strain softening effects

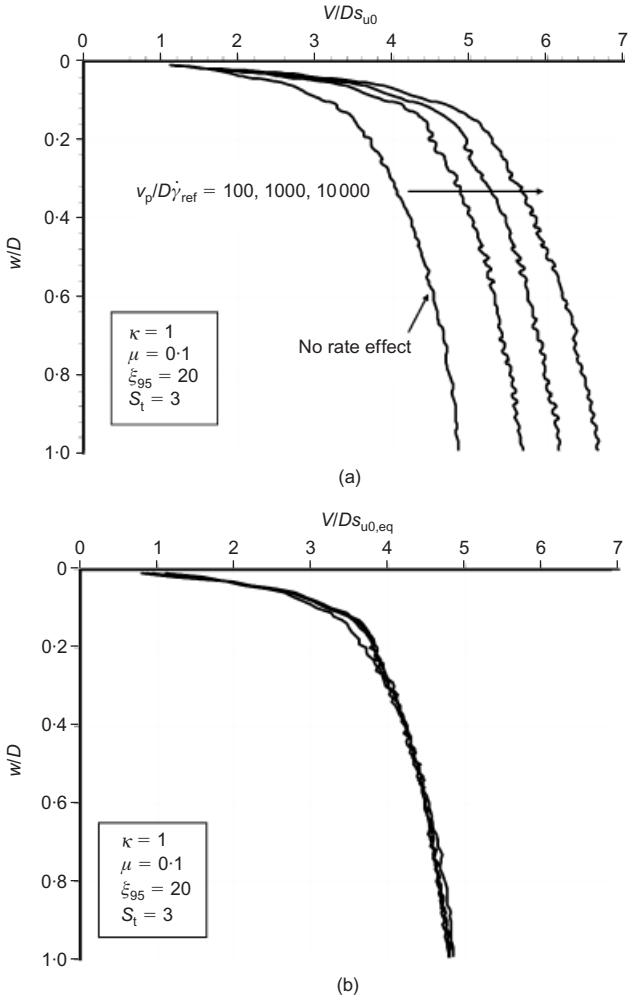

Fig. 7. Effect of normalised penetration rate on vertical resistance: (a) V normalised by original shear strength; (b) V normalised by equivalent shear strength

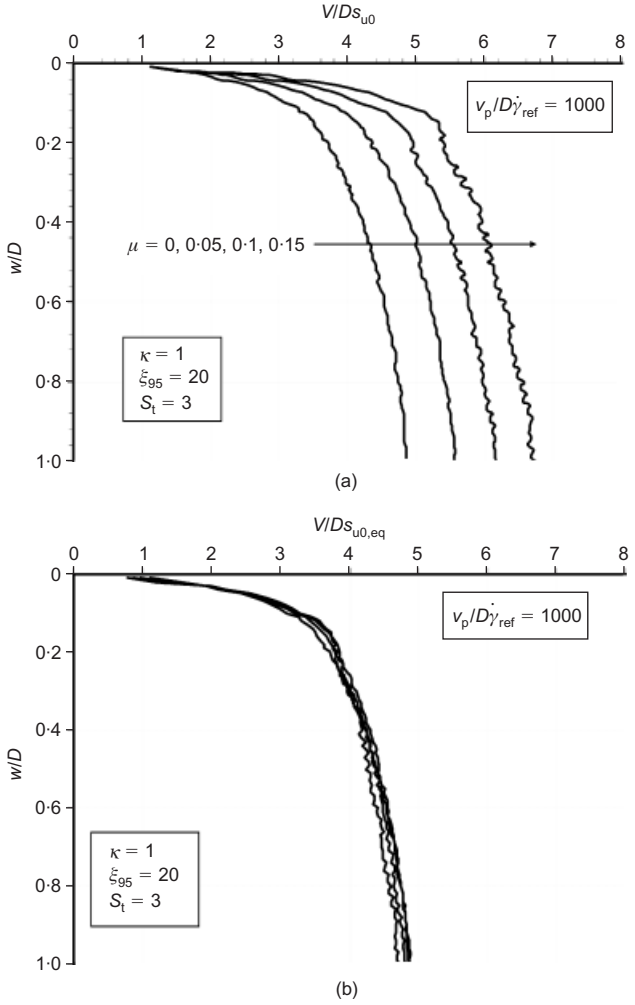

Fig. 8. Effect of rate parameter μ on vertical resistance: (a) V normalised by original shear strength; (b) V normalised by equivalent shear strength

normalised depth for different values of μ for $\kappa = 1$. The response for $\mu = 0$ is also included for purpose of comparison. In this case also, vertical resistance increased by more than 20% as μ was increased from 0·05 to 0·15. Normalising the vertical resistance by $s_{u0,eq}$, using equation (6) with $f_r = 0{\cdot}7$, all these curves fall in a narrow band (Fig. 8(b)).

Effect of sensitivity

The sensitivity of the soil causes the operative strength during pipe penetration to be lower than the original intact strength. Three values of sensitivity, $S_t = 2$, 3 and 6, were considered and other parameters for all these cases were kept equal to the base case. Higher sensitivity results in a higher rate of softening and lower penetration resistance. Fig. 9(a) shows variations of vertical resistance for different values of sensitivity for soil with $\kappa = 1$. Results for soil with no softening, that is a sensitivity of unity, are also shown in this figure. The vertical resistance reduces by more than 20% at shallow depths as the sensitivity increases from 1 to 6. In all cases, the interface resistance was taken as equal to the inverse of the sensitivity times the mudline shear strength (i.e. an interface resistance $= 0{\cdot}167s_{um}$, $0{\cdot}33s_{um}$, $0{\cdot}5s_{um}$ and s_{um} for sensitivity values of 6, 3, 2 and 1 respectively). If a single value of interface friction is used for all cases, corresponding to the base case value of $0{\cdot}33s_{um}$, the variation in vertical resistance is much less (as shown in Fig. 9(b)). This is because now there is only the effect of the change of sensitivity within the soil mass itself, while previously there was an additional effect of the interface initially being at the different values of fully remoulded strength, s_{um}/S_t.

To characterise the effect of the change in soil sensitivity, an equivalent shear strength was back-calculated as

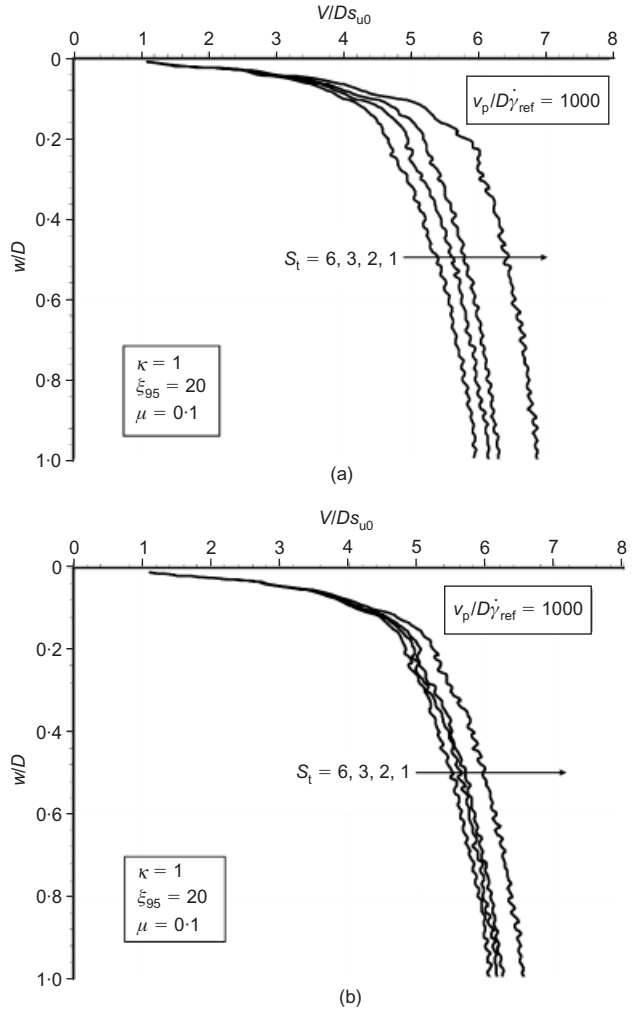

Fig. 9. Effect of sensitivity on vertical resistance: (a) $\alpha = 1/S_t$; (b) constant α (= 0·33)

$$s_{u,eq} = s_{u0}\left[\delta_{rem} + (1 - \delta_{rem})e^{-3f_s(w/D)/\xi_{95}}\right] \quad (7)$$

The term $f_s(w/D)$ in equation (7) reflects the equivalent plastic strain (proportional to w/D) undergone by the soil as it is deformed by the pipe. A value of 0·8 for the coefficient f_s was required to bring together the curves for the cases with different sensitivities and the same α (Fig. 10), implying that a representative operative strength during shallow pipe penetration is that at a plastic strain corresponding to 0·8w/D.

Effect of ductility parameter ξ_{95}

The value of the ductility parameter, ξ_{95}, was varied between 10, 20 and 30 to examine its effect on the vertical resistance, as shown in Fig. 11 for $\kappa = 1$. The penetration resistance increases by more than 10% as the soil becomes more ductile, with ξ_{95} increasing from 10 to 30. Vertical resistances were normalised using an equivalent shear strength based on equation (7) and a value of $f_s = 0{\cdot}8$, which brought all the curves of Fig. 11(a) together, as shown in Fig. 11(b).

Combining effects of strain rate and softening parameters

It may be seen from the above results that the strain rate and softening parameters have marked effects on the overall penetration response of pipelines. An attempt is made here to derive a single curve for the vertical penetration resistance with depth that accounts for the effects of all these parameters. The current practice is to unify the penetration response in soils of different strength profiles by normalising the vertical force by the shear strength of the soil at the invert of the pipe. In strain-rate-dependent, softening soil, this approach is extended by normalising the vertical resistance force by an equivalent shear strength of the soil at the

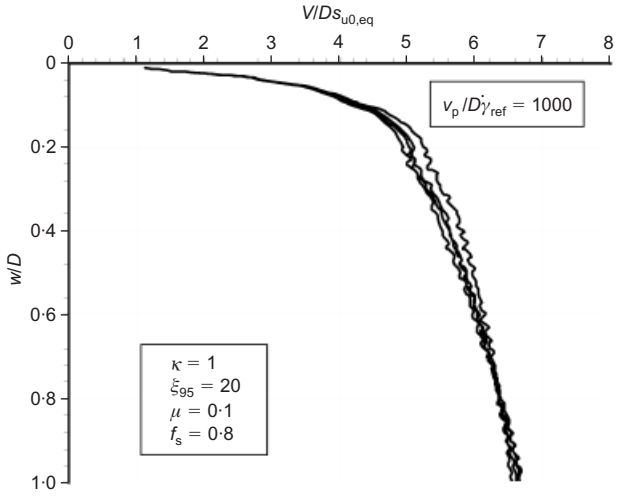

Fig. 10. Vertical resistances normalised by equivalent shear strength for different sensitivity values ($f_s = 0{\cdot}8$)

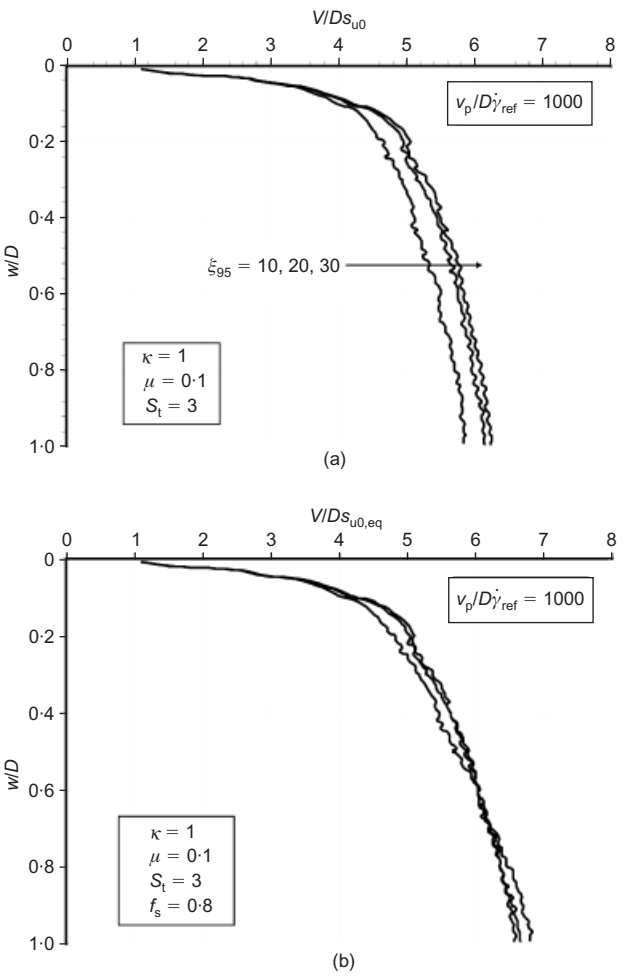

Fig. 11. Effect of ductility parameter ξ_{95} on vertical resistance: (a) V normalised by original shear strength; (b) V normalised by equivalent shear strength

pipe invert, incorporating the effects of strain rate and softening parameters. The equivalent shear strength, $s_{u0,eq}$ is expressed as

$$s_{u0,eq} = \left[1 + \mu \log\left(f_r v_p / D\dot{\gamma}_{ref}\right)\right] \left[\delta_{rem} + (1 - \delta_{rem})e^{(-3 f_s (w/D)/\xi_{95})}\right] s_{u0} \quad (8)$$

where f_r and f_s are the two constant factors introduced earlier and all other symbols are as in equation (1). The vertical resistance force, V, is normalised by $Ds_{u0,eq}$. For $\kappa = 1$, the vertical resistance normalised by the equivalent shear strength at the pipe invert was plotted in a single graph for all the cases of Table 1. It is seen from Fig. 12 that all the points fall into a narrow band when $f_r = 0{\cdot}7$ and $f_s = 0{\cdot}8$ are used. These sets of values can be fitted by power law curves of the form $V/Ds_{u0,eq} = a.(w/D)^b$, although two separate portions are required to provide a good fit, matching the curves at $w/D = 0{\cdot}1$. The best fits are expressed as

$$\frac{V}{Ds_{u0,eq}} = \left(\frac{V}{Ds_{u0,eq}}\right)_{w/D=0{\cdot}1} \left(10\frac{w}{D}\right)^{0{\cdot}5} \approx 3{\cdot}3\sqrt{10\frac{w}{D}} \quad \text{for } w/D \leqslant 0{\cdot}1$$

$$\frac{V}{Ds_{u0,eq}} = 5{\cdot}2\left(\frac{w}{D}\right)^{0{\cdot}19} \quad \text{for } w/D > 0{\cdot}1 \quad (9)$$

Effect of soil non-homogeneity

The power law equation fit stated above is fitted to the shear strength profile $\kappa = 1$. Two other shear strength profiles were considered: uniform soil with $\kappa = 0$ and soil with high shear strength gradient, $\kappa = 20$. The previous procedure described for $\kappa = 1$ was repeated for these two cases. For normalised displacement $w/D \geqslant 0{\cdot}1$, $V/Ds_{u0,eq} = a(w/D)^b$ equations were fitted and values of coefficients a and b were obtained. These coefficients, together with the value of $V/Ds_{u0,eq}$ at $w/D = 0{\cdot}1$, are tabulated in Table 3 for different values of κ. For $w/D \leqslant 0{\cdot}1$, the same curve as in equation (9) is used. The resulting curves are shown on Fig. 13.

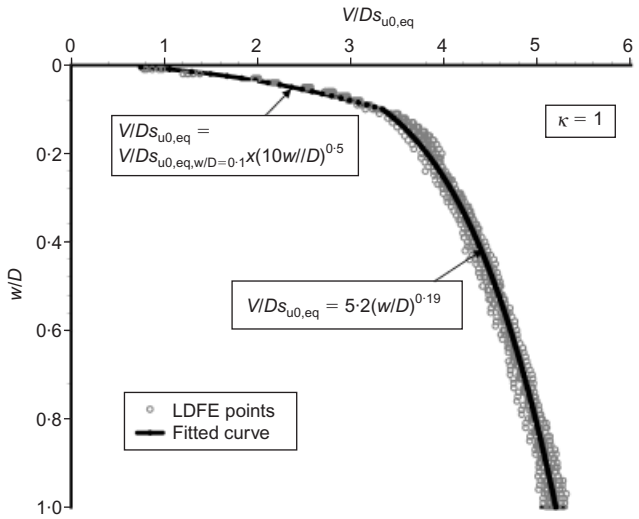

Fig. 12. Best-fit power law curve for vertical resistance with depth

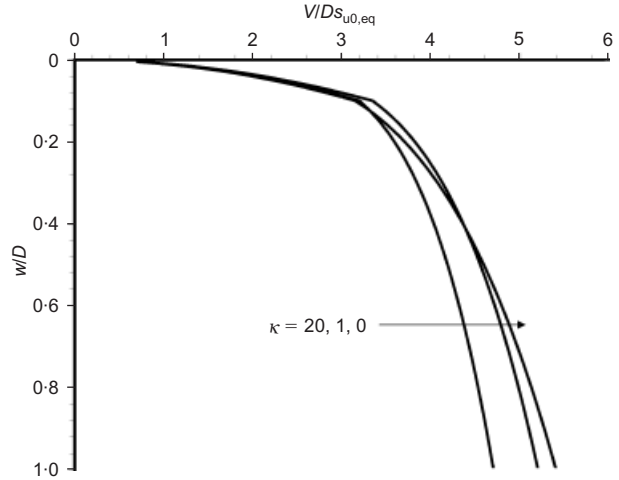

Fig. 13. Best-fit power law curves for vertical resistances for different κ

Table 3. Power law fit coefficient a and b for different shear strength profile

κ	a	b	$(V/Ds_{u0,eq})_{w/D=0{\cdot}1}$
0	5·4	0·23	3·18
1	5·2	0·19	3·35
20	4·7	0·17	3·18

Soil flow patterns

The main advantage of the present LDFE analysis is its ability to capture the changes in geometry and subsequent formation of heave when the pipe is pushed into the soil. It is of interest to consider the shape and size of the soil heave for different shear strength profiles, and also the soil flow mechanism during pipe penetration for different cases. These are illustrated for a normalised displacement $w/D = 0{\cdot}5$ in Fig. 14. It may be seen that for soil with low κ values, the mechanism is relatively deep and wide with the heave decaying gradually with distance from the pipe. On the other hand, for soil with high κ the mechanism is shallower – tending to favour the weaker shallower soil – and with the heave concentrated close to the pipe.

The taller heave profiles for $\kappa = 20$ illustrate why a higher enhancement of the soil buoyancy applies for this case (equation (5)). The net vertical displacement of soil displaced by the penetrating pipe is from the base of the pipe to the top of a high heave profile. This additional elevation beyond merely the original soil surface (for which $f_b = 1$) explains the higher buoyancy factor of 1·75 determined for $\kappa = 20$.

CONCLUDING REMARKS

The LDFE analysis approach described in this paper provides a more rigorous analysis for vertical penetration of seabed pipelines than other theoretical methods currently available in the literature. The method accounts for geometry changes in the surface of the seabed in the form of heave, and also the effects of strain rate and softening by modifying the simple linearly-elastic–perfectly-plastic Tresca soil model. Profiles of vertical penetration resistance with normalised displacement obtained from this study were compared with results from a centrifuge model test. Good agreement between these two results was obtained, supporting the validity of the finite-element approach.

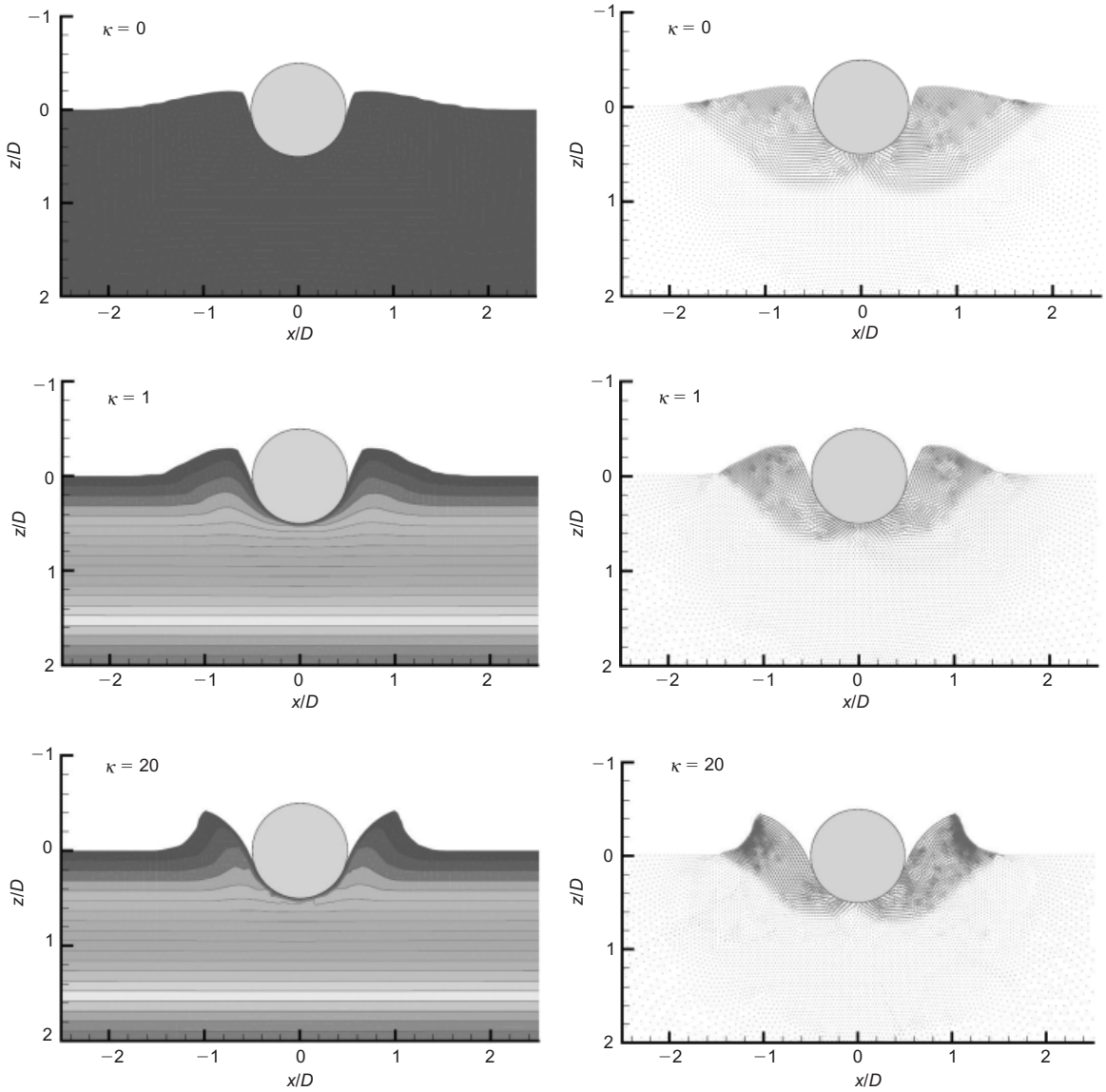

Fig. 14. Deformation pattern and instantaneous velocity field at $w/D = 0{\cdot}5$ for different κ

The shear strength was modified in each step of the LDFE analysis by multiplying it by two factors, accounting for

(*a*) enhancement of strength at increasing strain rates (relative to a reference value)
(*b*) softening as the soil is remoulded.

It was found that the strain rate and softening parameters have significant effect on the vertical resistance. However, it was found that normalising the vertical resistance by an equivalent shear strength, accounting for the strain rate and softening parameters, led to a narrow band of values when plotted against normalised penetration of the pipe. These sets of values were fitted by power law expressions, using different equations for $w/D \leqslant 0{\cdot}1$ and $w/D > 0{\cdot}1$.

The effect of buoyancy was also explored in this paper by varying the submerged unit weight of the soil. The total vertical resistance was divided into a geotechnical resistance (due to soil strength) and resistance due to soil buoyancy. Values for f_b (a multiplication factor on Archimedes' buoyancy) were provided for different strength profiles, refining the previous published value of 1·5.

The effect of soil non-homogeneity was also investigated in this paper, leading to different power law fit coefficients for soils with different shear strength profile, expressed as $\kappa = kD/s_{um}$. The heave patterns and associated soil flow kinematics were illustrated for different values of κ.

It should be noted that the present paper does not deal with excess embedment of pipes due to dynamic lay effects, which is a further important consideration in assessing the as-laid embedment of seabed pipelines. Another potential limitation of the present paper is the assumption of a constant pipe–soil interface shear strength, fixed as a fraction of the original mudline shear strength. In reality, the interface shear strength might be better modelled as a fraction of the remoulded shear strength of the surrounding soil, but experimental observations to resolve this are not available.

ACKNOWLEDGEMENTS

This work forms part of the activities of the Centre for Offshore Foundation Systems (COFS), established under the ARC Research Centres Program and now supported through Centre of Excellence funding from the State Government of Western Australia. Support is also acknowledged from the ARC Federation and Future Fellowships programmes and the ARC Discovery programme. The first author is supported by an international postgraduate research scholarship and a

university postgraduate research award from the University of Western Australia.

REFERENCES

Aubeny, C. P., Shi, H. & Murff, J. D. (2005). Collapse load for a cylinder embedded in trench in cohesive soil. *Int. J. Geomech*. **5**, No. 4, 320–325.

Biscontin, G. & Pestana, J. M. (2001). Influence of peripheral velocity on vane shear strength of an artificial clay. *Geotech. Test. J.* **24**, No. 4, 423–429.

Bruton, D. A. S., White, D. J., Cheuk, C. Y., Bolton, M. D. & Carr, M. C. (2006). Pipe–soil interaction behaviour during lateral buckling, including large amplitude cyclic displacement tests by the Safebuck JIP. *Proc. Offshore Technology Conf., Houston* paper OTC 17944.

Casagrande, A. & Wilson, S. D. (1951). Effect of rate of loading on the strength of clays and shales at constant water content. *Géotechnique* **2**, No. 3, 251–263, http://dx.doi.org/10.1680/geot.1951.2.3.251.

Dassault Systèmes (2007). *Abaqus analysis users' manual*. Providence, RI, USA: Simula Corp.

Dingle, H. R. C., White, D. J. & Gaudin, C. (2008). Mechanisms of pipe embedment and lateral breakout on soft clay. *Can. Geotech. J.* **45**, No. 5, 636–652.

Einav, I. & Randolph, M. F. (2005). Combining upper bound and strain path methods for evaluating penetration resistance. *Int. J. Numer. Methods Engng* **63**, No. 14, 1991–2016.

Ghosh, S. & Kikuchi, N. (1991). An arbitrary Lagrangian–Eulerian finite element method for large deformation analysis of elastic-viscoplastic solids. *Comput. Methods Appl. Mech. Engng* **86**, No. 2, 127–188.

Graham, J., Crooks, J. H. A. & Bell, A. L. (1983). Time effects on the stress–strain behaviour of natural soft clays. *Géotechnique* **33**, No. 3, 327–340, http://dx.doi.org/10.1680/geot.1983.33.3.327.

Hu, Y. & Randolph, M. F. (1998a). A practical numerical approach for large deformation problems in soil. *Int. J. Numer. Analyt. Meth. Geomech*. **22**, No. 5, 327–350.

Hu, Y. & Randolph, M. F. (1998b). *H*-adaptive FE analysis of elastoplastic non-homogeneous soil with large deformation. *Comput. Geotech*. **23**, No. 1–2, 61–83.

Lefebvre, G. & LeBoeuf, D. (1987). Rate effects and cyclic loading of sensitive clays. *J. Geotech. Engng* **113**, No. 5, 476–489.

Low, H. E., Randolph, M. F., DeJong, J. T. & Yafrate, N. J. (2008). Variable rate full-flow penetration tests in intact and remoulded soil. *Proc. 3rd Int. Conf. on Geotech. Geophys. Site Characterization, Taipei, Taiwan* 1087–1092. London, UK: Taylor and Francis Group.

Lunne, T. & Andersen, K. H. (2007). Soft clay shear strength parameters for deepwater geotechnical design. *Proc. 6th Int. Offshore Site Investigation Geotech. Conf.: Confronting New Challenges and Sharing Knowledge* **1**, 151–176. London, UK: Society for Underwater Technology.

Lunne, T., Berre, T., Andersen, K. H., Strandvik, S. & Sjursen, M. (2006). Effects of sample disturbance and consolidation procedures on measured shear strength of soft marine Norwegian clays. *Can. Geotech. J.* **43**, No. 7, 726–750.

Martin, C. M. & Randolph, M. F. (2006). Upper bound analysis of lateral pile capacity in cohesive soil. *Géotechnique* **56**, No. 2, 141–145, http://dx.doi.org/10.1680/geot.2006.56.2.141.

Merifield, R. S., White, D. J. & Randolph, M. F. (2008). The ultimate undrained resistance of partially embedded pipelines. *Géotechnique* **58**, No. 6, 461–470, http://dx.doi.org/10.1680/geot.2007.00097.

Merifield, R. S., White, D. J. & Randolph, M. F. (2009). Effect of surface heave on response of partially embedded pipelines on clay. *J. Geotech. Geoenviron. Engng, ASCE* **135**, No. 6, 819–829.

Murff, J. D., Wagner, D. A. & Randolph, M. F. (1989). Pipe penetration in cohesive soil. *Géotechnique* **39**, No. 2, 213–229, http://dx.doi.org/10.1680/geot.1989.39.2.213.

Randolph, M. F. (2004). Characterization of soft sediments for offshore applications. Keynote lecture. *Proc. 2nd Int. Conf. on Site Characterization, Porto, Portugal* **1**, 209–231. Rotterdam, The Netherlands: Millpress Science Publishers.

Randolph, M. F. & Houlsby, G. T. (1984). The limiting pressure on a circular pile loaded laterally in cohesive soil. *Géotechnique* **34**, No. 4, 613–623, http://dx.doi.org/10.1680/geot.1984.34.4.613.

Randolph, M. F. & White, D. J. (2008a). Offshore foundation design – a moving target. *Proceedings of the BGA international conference on foundations*, Dundee, pp. 27–59. London, UK: IHS BRE Press.

Randolph, M. F. & White, D. J. (2008b). Pipeline embedment in deep water: process and quantitative assessment. *Proceedings of the offshore technology conference*, Houston, paper OTC 19128.

Randolph, M. F. & White, D. J. (2008c). Upper-bound yield envelopes for pipelines at shallow embedment in clay. *Géotechnique* **58**, No. 4, 297–301, http://dx.doi.org/10.1680/geot.2008.58.4.297.

Verley, R. & Lund, K. M. (1995). A soil resistance model for pipelines placed on clay soils. *Proc. ASME Int. Conf. Offshore Mech. Arctic Engng, Copenhagen* **5**, 225–232.

Wang, D., White, D. J. & Randolph, M. F. (2010). Large deformation finite element analysis of pipe penetration and large-amplitude lateral displacement. *Can. Geotech. J.* **47**, No. 8, 842–856.

Yafrate, N. J. & DeJong, J. T. (2007). Influence of penetration rate on measured resistance with full-flow penetrometers in soft clay. *Proceedings of GeoDenver 2007 – Advances in measurement and modelling of soil behaviour, ASCE*, GSP No. 173.

Zhou, H. & Randolph, M. F. (2007). Computational techniques and shear band development for cylindrical and spherical penetrometers in strain-softening clay. *Int. J. Geomech*. **7**, No. 4, 287–295.

Zhou, H. & Randolph, M. F. (2009). Resistance of full-flow penetrometers in rate-dependent and strain-softening clay. *Géotechnique* **59**, No. 2, 79–86, http://dx.doi.org/10.1680/geot.2007.00164.

Zienkiewicz, O. C. & Zhu, J. Z. (1992). The superconvergent patch recovery and posterior error estimates. Part 1: The recovery technique. *Int. J. Numer. Meth. Engng* **33**, No. 7, 1331–1364.